Article ID: 1000-324X(2023)12-1466-09 **DOI:** 10.15541/jim20230215

Jointing of Cathode Coating and Interface Modification for Stabilizing Poly(ethylene oxide) Electrolytes Against High-voltage Cathodes

TAN Shuyu, LIU Xiaoning, BI Zhijie, WAN Yong, GUO Xiangxin

(College of Physics, Qingdao University, Qingdao 266071, China)

Abstract: Poly(ethylene oxide) (PEO)-based solid electrolytes are deemed as the most promising alternatives for solid-state lithium batteries on account of their low cost, good stability against Li metal, and easy large-scale production. However, the instability of PEO against high-voltage cathodes severely limits its application in the fields needing high energy density. In this work, a discontinuous cyclized polyacrylonitrile (cPAN) nanolayer, served as an electron-conducting shell, is partially coated on $LiNi_{0.6}Co_{0.2}Mn_{0.2}O_2$ (NCM) cathode particles, while an ionic liquid acted as ion-conducting pathway is introduced at NCM/PEO interface, enabling the high compatibility of PEO against high-voltage NCM cathode. The cPAN layer not only physically isolates the direct contact of PEO electrolyte from NCM cathode, but also contributes to the electronic transfer inside the cathode due to the formation of delocalized sp^2 π bond during coating process. Meanwhile, the mobile ionic liquid with good ionic conductivity fully wets cathodic interface, followed by decomposition into cathode-electrolyte interphase (CEI) of LiF and Li_3N, further restricting the oxidation-failure of PEO electrolyte. By taking the combined strategy, the corresponding solid-state NCM/Li battery delivers an excellent electrochemical performance with a capacity retention of 85.3% after 100 cycles at rate of 0.1*C* (1*C*=0.18 $A\cdot g^{-1}$) under a cutoff voltage of 4.30 V. This work opens up a new direction to address the interfacial stability issues of PEO-based electrolyte against high-voltage cathodes through surface coating and interface modification.

Key words: poly(ethylene oxide); cyclization; high-voltage cathode; interface engineering; solid-state lithium battery

Rechargeable lithium (Li) metal battery is the most promising energy-storage device because of its high specific capacity and long cycling life[1-3]. However, limited by the flammability of organic liquid electrolytes[4] and the growth of Li dendrites[5-6], the conventional Li metal batteries based on liquid electrolytes bring out a considerable safety hazard[7-8]. Therefore, the solid-state lithium batteries (SSLBs) have been proposed by replacing organic liquid electrolytes with non-combustible solid electrolytes, which can not only address the flammability issues[9], but also prevent electrolyte leakage and physically inhibit the growth of Li dendrite[10-12]. Until now, the solid electrolytes can be classified into two categories: inorganic ceramic electrolytes, and solid polymer electrolytes[13]. Among them, the polymer electrolytes based on poly(ethylene oxide) (PEO) have been used in the commercialization of practical solid-state batteries due to their advantages of light weight, low cost, high flexibility, relative stability against Li metal, and solvated Li salts[14-17].

The most critical issue faced by PEO-based electrolyte focuses on the narrow electrochemical window below 4 V (*vs* Li/Li^+)[18], confining its compatibility with only low-voltage $LiFePO_4$ (LFP) cathodes[19]. This is due to the oxidation of terminal hydroxide (–OH) group and main chain (C–O–C) of PEO under the condition of high voltage[20]. Considering such continuous oxidation, PEO-based electrolytes seem impossible to be paired with high-voltage cathodes, such as $LiCoO_2$ (LCO)[21-22] and $LiNi_xCoyMn_{1-x-y}O_2$[23-24], which is detrimental to the realization of high energy density. In order to suppress the oxidation of PEO under high voltage, a great many

Received date: 2023-05-05; **Revised date:** 2023-06-25; **Published online:** 2023-07-28
Foundation item: National Natural Science Foundation of China (22005163, U1932205); Natural Science Foundation of Shandong Province (ZR2020MA084); Key R&D Program of Shandong Province (2021CXGC010401); Taishan Scholars Program (ts201712035)
Biography: TAN Shuyu (1998–), female, Master candidate. E-mail: tsy1576362772@163.com
谭淑雨(1998–), 女, 硕士研究生. E-mail: tsy1576362772@163.com
Corresponding author: WAN Yong, professor. E-mail: wanyongqd@hotmail.com; GUO Xiangxin, professor. E-mail: xxguo@qdu.edu.cn
万 勇, 教授. E-mail: wanyongqd@hotmail.com; 郭向欣, 教授. E-mail: xxguo@qdu.edu.cn

strategies have been carried out. Coating the high-voltage cathodes with protective shells has been proved to be an effective means to isolate PEO electrolytes from direct contact with cathodes, inhibiting oxidation of PEO at high charging potential[25-27]. However, the unchanged poor interfacial contact between cathode and PEO electrolyte limits the interfacial transfer of Li^+, bringing an insufficient capacity and cycling stability[28]. In addition, the asymmetric configurations of polymer electrolytes by constructing oxidation-resistance intermediate layers[29], like succinonitrile (SN), polyvinylidene fluoride (PVDF), polyacrylonitrile (PAN), *etc.*, between high-voltage cathodes and PEO electrolytes also effectively address the electrochemical oxidation issue of PEO. However, the multilayered configuration leads to the enlarged thickness of solid electrolyte, limiting the volumetric energy density of SSLBs. Therefore, it remains a challenge to put forward a facile strategy to realize high compatibility of PEO electrolytes against high-voltage cathodes.

Herein, in order to address the compatibility of PEO-based electrolyte with high-voltage $LiNi_{0.6}Co_{0.2}Mn_{0.2}O_2$ (NCM) cathode, the cyclized polyacrylonitrile (cPAN) nanolayer with electronic transfer capability is partially coated on NCM particles (NCM@cPAN). As is well-known, the polyacrylonitrile (PAN) suffers from cyclization process at the temperature range of 200–400 ℃ in the air, leading to the generation of delocalized sp^2 π electrons for a certain electronic conductivity without losing its polymeric property of satisfactory mechanical resiliency[30]. Besides, the cPAN layer also plays a role of protective shell to isolate the direct contact of PEO with NCM particles. Furthermore, the mobile *N*-methyl-*N*-propylpiperidinium bis(trifluoromethanesulfonyl)imide (PP13-TFSI) based ionic liquid (IL) is introduced between NCM cathode plate and PEO electrolyte, inducing an intimate cathode/electrolyte interface for smooth Li^+ transfer. Subsequently, the rigid cathode-electrolyte-interphase (CEI) layer consisting of LiF and Li_3N forms during cycling, further separating NCM particles from PEO electrolyte and thus suppressing the oxidation of PEO. Therefore, by this means, the enhanced stability of PEO against high-voltage cathodes can be achieved with improved cycling and rate performance.

1 Experimental

1.1 Preparation of NCM@cPAN powder

The PAN (M_w=150,000) was uniformly dissolved in *N*, *N*-dimethylformamide (DMF) by vigorous stirring at 70 ℃. The NCM cathode powder was added in the above solution (1.5%(in mass) PAN) along with vigorous stirring at 70 ℃ for 0.5 h. Afterwards, the mixture was further dispersed by ultrasound for 10 min. The continuous stirring was taken at 100 ℃ until most of the solvent was evaporated. Then, the mixture was dried at 120 ℃ to completely remove the residual DMF solvent. Finally, the obtained composite powder was ground, followed by sintering at 400 ℃ for 0.5 h in the air to obtain the NCM@cPAN powder for later use. The schematic diagrams of preparation and structure of NCM@cPAN composite particles are shown in Fig. 1(a, b).

1.2 Preparation of PEO-based solid polymer electrolytes

PEO (M_w=100,000) and lithium bis (trifluoromethosulfonyl) imide (LiTFSI) with EO/Li of 16 : 1 (in molar) were dissolved in acetonitrile (ACN) by stirring at room temperature for 6 h. Then, the above viscous slurry was cast on both sides of cellulose separator with a doctor blade, followed by drying at 60 ℃ for 24 h to remove the ACN solvent. The obtained PEO electrolyte was punched into disk with the diameter of 19 mm for later use.

1.3 Material characterization

The X-ray diffraction (XRD, Bruker D8 Advance) was used to detect the phase structures of samples with Cu $K_{\alpha 1}$ radiation (λ=1.5406 Å) in the 2θ range of 10°~80°. The morphology and composition were obtained by scanning electron microscope (SEM, Hitachi S-4800), and transmission electron microscope (TEM, JEM-2100F) equipped with an energy dispersive X-ray spectroscopy (EDS). The chemical bonding species of PAN and PEO were obtained by Fourier infrared spectroscopy (FT-IR, Lambda Scientific FTIR-7600 spectrometer). The Raman spectroscopy was performed by using a Thermo Fischer DXR spectrometer to confirm the chemical situations of PAN and cPAN.

1.4 Assembly and electrochemical measurements of batteries

The ionic conductivity of PEO electrolyte was measured by a Princeton electrochemical workstation in a frequency range from 7 MHz to 0.1 Hz with symmetric stainless steel (SS) blocking electrodes. The electrochemical window was tested using the linear sweep voltammetry (LSV) measurement with a scanning rate of 0.001 $V \cdot s^{-1}$. The cathode plate was prepared by casting the uniform slurry consisted of NCM@cPAN particles, carbon black and polyvinylidene fluoride (PVDF) binder in *N*-methyl pyrrolidone (NMP) solvent with a weight ratio of 80 : 10 : 10 on Al foil. The cathode plate was then heated at 80 ℃ overnight to remove the NMP solvent. The ionic liquid was prepared by uniformly dissolving 0.2 $mol \cdot L^{-1}$ LiTFSI into *N*-methyl-*N*-propylpiperidinium bis(trifluoromethanesulfonyl)imide (PP13-TFSI). The

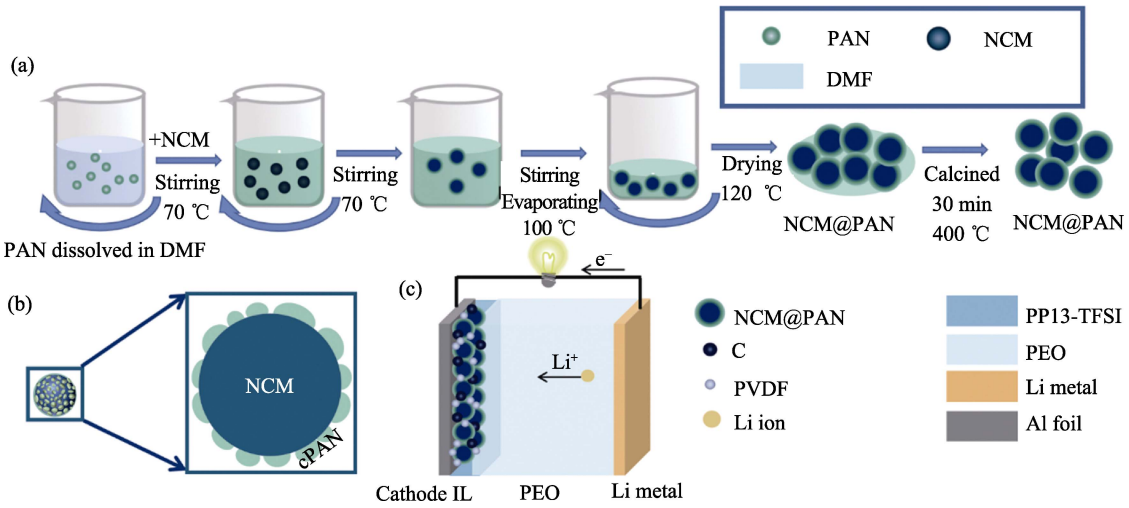

Fig. 1 (a) Preparation process of NCM@cPAN powder, (b) schematic representation of as-prepared NCM@cPAN particle, and (c) schematic diagram of the solid-state NCM@cPAN+IL/PEO/Li cell

2032-type coin cells were assembled by integrating NCM@cPAN cathode, PEO solid electrolyte and Li-metal anode in an Ar-filled glove box (Mikrouna) with O_2 and H_2O contents below 0.1 $\mu L \cdot L^{-1}$. 2 μL IL was introduced at the interface between NCM@cPAN cathode and PEO electrolyte. The cell configuration is schematically presented in Fig. 1(c). Besides, the solid-state batteries based on pristine NCM cathode without IL, and NCM@cPAN cathode without IL were assembled for comparison. The galvanostatic charge-discharge tests were carried out using Land CT2001A cycler within the cutoff potentials of 4.20, 4.25 and 4.30 V (*vs* Li^+/Li). All electrochemical measurements were carried out at 50 ℃.

2 Results and discussion

2.1 Characterization of NCM@cPAN powders

Fourier transform infrared spectroscopy (FT-IR) spectra of PAN powders without and with heat-treatment at 400 ℃ are shown in Fig. 2(a). The absorption peaks located at 2238, 1449 and 1365 cm^{-1} for pristine PAN are respectively corresponding to –C≡N, $–CH_2$ and –CH groups[31]. In terms of cPAN with heat-treatment at 400 ℃ for 30 min, the peak at 2238 cm^{-1} is absent, indicating that the characteristic –C≡N group is damaged. Instead, the newly appeared peak at 1570 cm^{-1} indicates the formation of C=N groups for cPAN molecule. This transformation is attributed to the opening of C≡N at elevated temperature for PAN, leading to the formation of cyclized PAN. As can be seen from Fig. 2(b), N of cyano group in pristine PAN is converted into pyridinic-N in cPAN during the cyclization process. Such cyclized structure possesses delocalized sp^2 π electrons through the whole molecular structure, endowing cPAN with certain electronic conductivity. Furthermore, Raman measurements were taken to acquire direct evidence to confirm the presence of delocalized π bonds in cPAN molecule, as displayed in Fig. 2(c). D and G peaks located at 1596 and 1374 cm^{-1} in Raman spectrum of cPAN confirm the existence of delocalized sp^2 π bonds and thus the electronic transfer

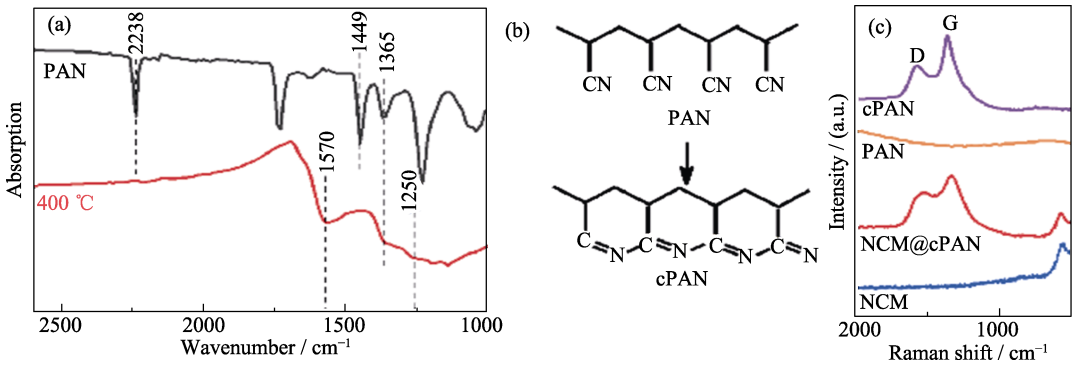

Fig. 2 (a) FT-IR spectra of pristine PAN and PAN treated at 400 ℃, (b) schematic diagrams of pristine PAN and cPAN, and (c) Raman spectra of PAN, cPAN, NCM, and NCM@cPAN

capability of cPAN. Similarly, as indicated in Fig. 2(c), the bare NCM shows a single peak at ~550 cm^{-1}, while NCM@cPAN exhibits a pair of D and G peaks in addition to the characteristic peak of NCM at ~550 cm^{-1}[32-33]. Therefore, the NCM particles are well integrated with cPAN coating layer, which helps to improve the electronic transfer capability of the composite cathode materials.

The structural characterization of NCM@cPAN is presented in Fig. 3. Fig. 3(a) shows XRD patterns of NCM, NCM@PAN and NCM@cPAN powders. It can be found that the characteristic peaks of NCM cathode particles exhibit no change during the coating process, along with no generation of additional impurity peaks.

SEM was used to investigate the morphologies of NCM particles at different stages during the coating process. The pristine NCM is a large spherical agglomerate made up of a large number of small primary particles (Fig. 3(b, c)). Comparatively, a coating layer is covered on NCM surface for both NCM@PAN (Fig. 3(d, e)) and NCM@cPAN (Fig. 3(f, g)) powders. Certainly, the morphology difference between NCM@PAN and NCM@cPAN lies in the varying heating treatments. In addition, the element mappings in Fig. 3(j) show distributions of C, N, and O, suggesting the homogenous distribution of cPAN layer on NCM surface. Furthermore, TEM images confirm the partially polymer coating layers on NCM particles for NCM@cPAN (Fig. 3(h, i)). Such cPAN layer has a certain electronic conductivity and mechanical resiliency, enabling the electronic transfer inside the cathode and the enhanced stability of NCM cathode.

2.2 Electrochemical performance of PEO-based solid-state batteries with NCM@cPAN cathodes and IL modification

To evaluate the effect of the proposed interface engineering strategy on the long-term cycling stability of PEO-based electrolytes, the full cells were assembled using NCM@cPAN cathodes, PEO-based electrolytes, and Li-metal anodes. Besides, a trace amount of IL was introduced between the cathode and PEO electrolyte for smooth Li^+ transfer at cathode/PEO interface. Fig. S1(a) shows Nyquist plots of PEO-LiTFSI electrolytes under different testing temperatures, where the PEO based electrolyte exhibits an ionic conductivity of 3.75×10^{-5} S·cm^{-1} at 30 ℃. The corresponding activation energy of PEO electrolyte is ~0.42 eV, which can be calculated from the fitted Arrhenius plot shown in Fig. S1(b). In addition, the linear sweep voltammetry (LSV) curve of PEO electrolyte is presented in Fig. S2, in which a quite narrow potential window of ~3.8 V is detected due to the oxidation of terminal –OH group and main chain of PEO. Profited by the combination of cPAN coating layer and IL modification, the solid-state cell delivers an initial discharge capacity of 153 mAh·g^{-1}, accompanied with a capacity retention of 88.0% after 100 cycles under the cutoff voltage of 4.20 V (Fig. 4(a, d)). The analogical

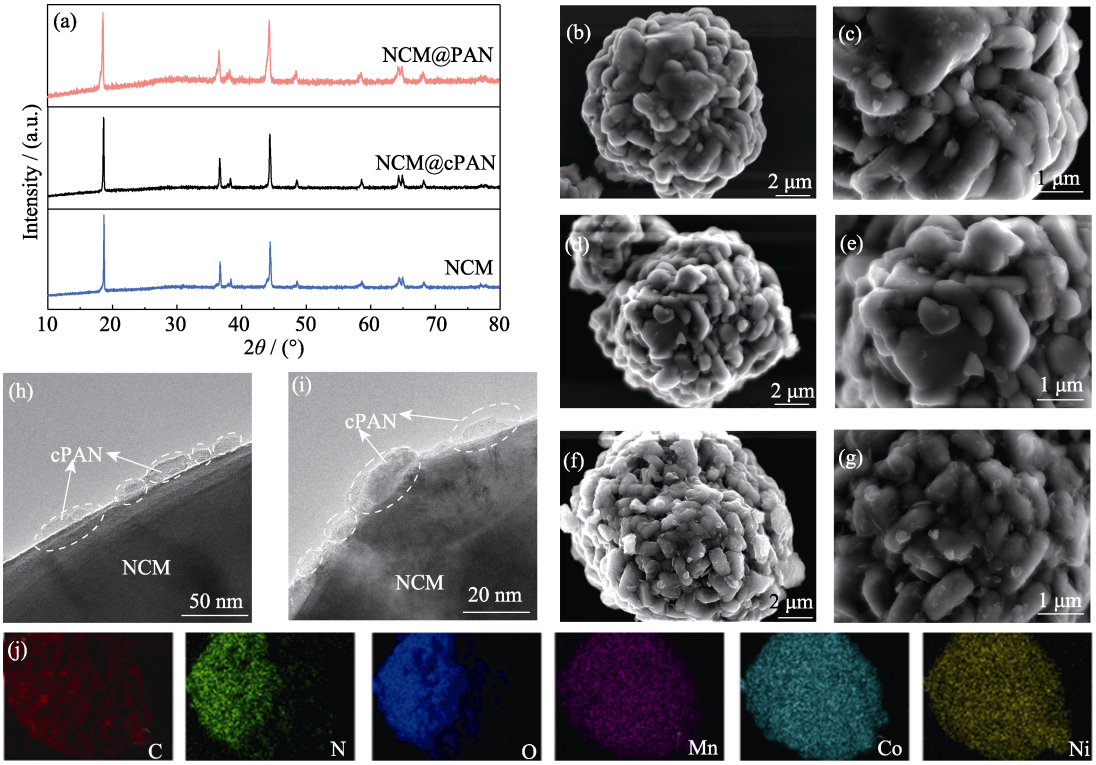

Fig. 3　(a) XRD patterns of NCM, NCM@PAN, and NCM@cPAN powders; SEM images of (b, c) NCM, (d, e) NCM@PAN, and (f, g) NCM@cPAN powders; (h, i) TEM images of NCM@cPAN; (j) EDS mappings of C, N, O, Mn, Co and Ni elements of the region in (f)

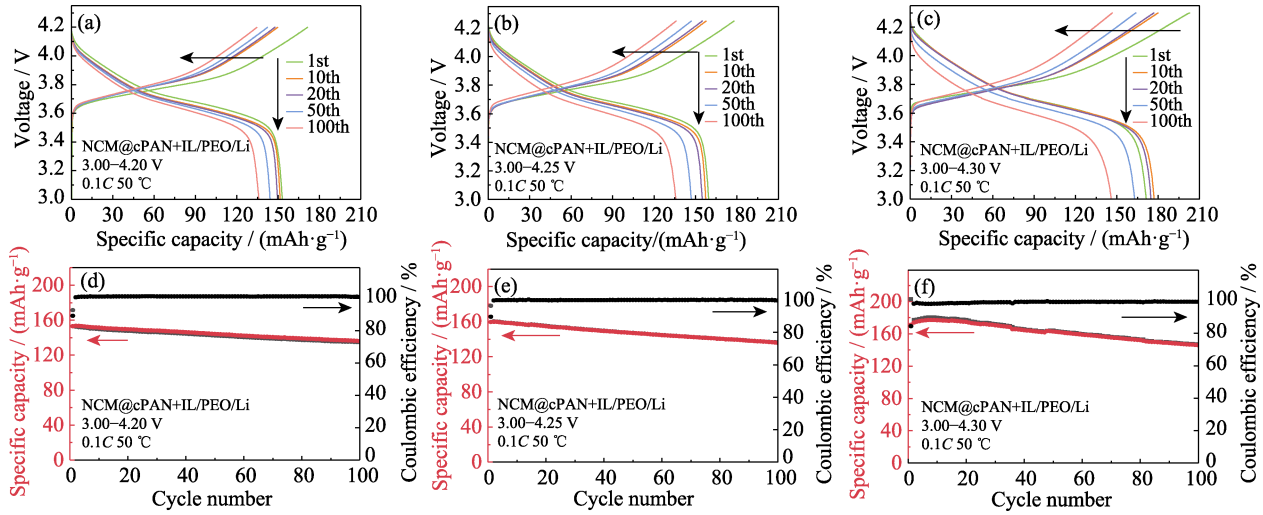

Fig. 4 Cycling performance of solid-state NCM@cPAN+IL/PEO/Li batteries

Typical charge-discharge curves and the corresponding specific capacities with cutoff voltages of (a, d) 4.20 V, (b, e) 4.25 V, and (c, f) 4.30 V

results are obtained in terms of the charging cutoff voltages increasing up to 4.25 and 4.30 V. Specifically, an initial discharge capacity of 159 mAh·g^{-1} is acquired for the solid-state cell based on NCM@cPAN cathode, followed by a capacity retention of 85.2% after 100 cycles under a cutoff voltage of 4.25 V, as shown in Fig. 4(b, e). Meanwhile, the modified NCM@cPAN cathode is also compatible with higher charging cutoff voltage of 4.30 V, as indicated in Fig. 4(c), where an initial discharge capacity of 171 mAh·g^{-1} is obtained, along with the good shapes of charge-discharge curves during the whole cycling. In addition, a satisfactory capacity retention of 85.3% is detected under the cutoff voltage of 4.30 V, as shown in Fig. 4(f). It is worth noting that the average Coulombic efficiency of NCM@cPAN based cell maintains higher than 99% during the whole cycling no matter for the cutoff voltages of 4.20, 4.25 or 4.30 V. This suggests the inhibited oxidation of PEO at high charging voltages due to the isolation of PEO from NCM cathode particles. In contrast, the solid-state cell based on pristine NCM without IL cannot normally work during the 4th cycle, because the transition metal ions including Ni^{3+}, Co^{3+}, and Mn^{4+} in high-valence states catalyze the oxidation of PEO due to the direct contact between NCM and PEO, as shown in Fig. S3.

The rate performance of solid-state NCM@cPAN+IL/PEO/Li batteries with dual-strategy modification was further investigated, as shown in Fig. 5. Fig. 5(a) displays the charge-discharge curves of NCM@cPAN+IL/PEO/Li cell at different current densities, in which all curves sustain the normal shapes with acceptable polarizations. The battery delivers a discharge capacity of 106.6 mAh·g^{-1} at rate of 0.5*C* (1*C*=0.18 A·g^{-1}), 70.4% of the value for 0.1*C* (151.5 mAh·g^{-1}). In addition, when the current density returns back to 0.1*C*, the specific discharge capacity can reach 150.1 mAh·g^{-1}, proving its superior rate performance, as shown in Fig. 5(b). Similar results are obtained based on the charge cutoff voltage increased to 4.25 and 4.30 V, as shown in Fig. S4. Such superior rate performance can be attributed to the composite ionic-electronic conducting networks in the cathode derived from the cPAN coating and IL penetration, as well as the smooth Li^+ transfer at cathode/electrolyte interface due to the wetting of IL.

To verify the feasibility of our strategy on solid-state batteries with higher cathode loading, the solid-state NCM@cPAN+IL/PEO/Li cell with a high cathode loading of ~6.2 mg·cm^{-2} was further assembled. A remarkable areal capacity of 0.91 mAh·cm^{-2} (corresponding to 146.1 mAh·g^{-1}) is achieved, together with a high capacity retention of 86.2% after 50 cycles at 0.1*C* (Fig. 5(c, d)). Thanks to the separation effect of cPAN layer, the oxidation of PEO is effectively suppressed during the cycling process even under the situation of high cathode mass loading.

The behavior of PP13-TFSI based ionic liquid during cycling was further analyzed by XPS measurement. For the as-prepared cathode/PEO interface with PP13-TFSI ionic liquid, the peak at 688.1 eV stands for –CF_3 group in $TFSI^-$, as shown in Fig. 6(a). The generation of LiF at 684.0 eV can be observed after cycling due to the decomposition of $TFSI^-$ anion (Fig. 6(c))[34]. In Fig. 6(b), the peaks located at 402.0 and 399.0 eV are respectively associated with N in $PP13^+$ cations and $TFSI^-$ anion[35]. After cycling, a new peak appears at 397.0 eV, which denotes the formation of Li_3N during cycling (Fig. 6(d))[36]. It can be found from XPS results that the ionic conducting cathode-electrolyte-interphase (CEI) layer made up of LiF and Li_3N is generated at cathode/PEO interface, which further isolates the high-voltage NCM from PEO electrolyte

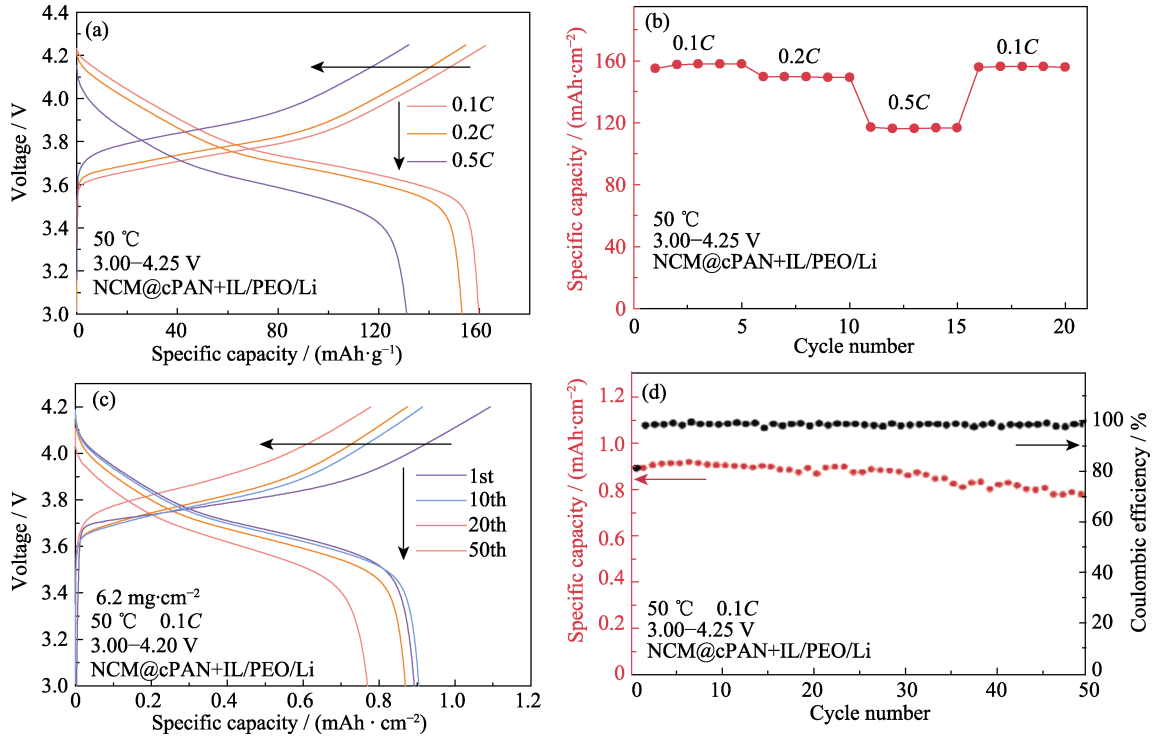

Fig. 5　(a) Charge-discharge curves, and (b) corresponding specific capacities for solid-state NCM@cPAN+IL/PEO/Li batteries at various current densities; (c) Typical charge-discharge curves and (d) corresponding specific capacities and Coulombic efficiency for solid-state NCM@cPAN+IL/PEO/Li batteries with high cathode loading of ~6.2 mg·cm^{-2}

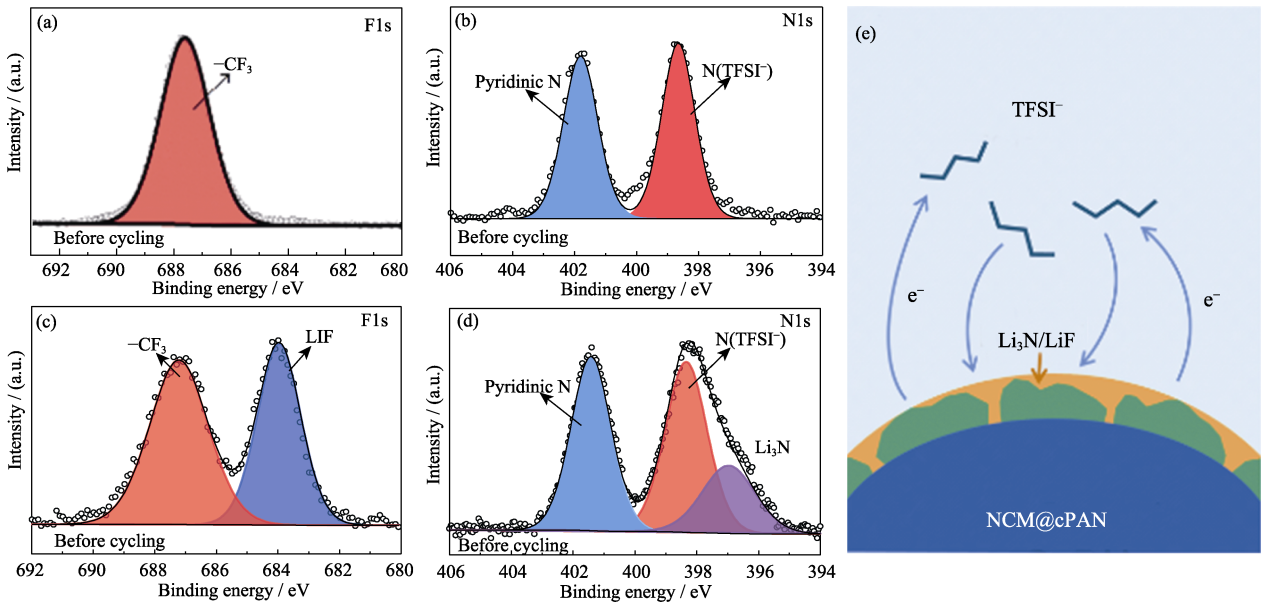

Fig. 6　(a, c) F1s and (b, d) N1s XPS spectra of PP13-TFSI (a, b) before and (c, d) after cycling; (e) Schematic diagram of TFSI$^-$ decomposition during cycling

for the reinforced stability of PEO, as shown in Fig. 6(e)[37-38]. Besides, the *in-situ* formed CEI also ensures the intimate cathode/electrolyte contact, and contributes to the smooth Li^+ transfer across the cathode/electrolyte interface, enabling the long-term stability of PEO based high-voltage SSLBs. By comparison, the direct coupling of NCM@cPAN cathode with PEO electrolyte but without the IL modification also cannot completely restrict the oxidation of PEO, as confirmed in Fig. S5, where the corresponding cell can only normally work within 10 cycles. This may be caused by the residual sites of NCM surface uncovered by cPAN coating, still inducing the direct contact of NCM and PEO and thus leading to the oxidation of PEO when charging at high potential. Analogously, the NCM/PEO/Li cell with IL modification but without

cathode coating also leads to the cell failure within 5 cycles (Fig. S6), which can be attributed to the unformed CEI at the initial stage of cycling and the soft nature of liquid, that cannot adequately isolate the contacting of PEO from high- voltage NCM cathode.

In our proposal, the discontinuous coating of cPAN and IL interface modification are combined to improve the stability of PEO electrolyte toward high-voltage cathode. Compared with the continuous cPAN coating layer owning electronic conductivity that restricts the effective ionic transfer inside the cathode, the discontinuous cPAN coating offers the pathway for electronic transfer, as well as leaves enough sites for the filling of IL and CEI with ionic conductivity during cycling. In this way, the jointing of cPAN coating and IL interface modification not only contributes to the transfer of both ions and electrons, but also effectively isolates the direct contact between NCM cathode and PEO electrolyte, realizing the improved stability of PEO electrolytes against high-voltage cathodes and thus the enhanced battery performance.

The FT-IR measurement was taken to evaluate the stability of PEO towards high-voltage cathode, as shown in Fig. 7(a). The characteristic peaks of pristine PEO electrolyte respectively refer to the triple peaks near 1100 cm^{-1} and the double peaks around 1350 cm^{-1}. Specifically, the peaks at 1343 cm^{-1} are related to the bending vibration peaks of $–CH_2$, while the peaks at 1145, 1095 and 1053 cm^{-1} correspond to the tensile peaks of C–O–C at main chain and the stretching vibration of C−O bond at the terminal C−OH alcohol group[39]. Such double and triple peaks confirmed the existence of PEO crystallinity. It can be seen from Fig. 7(a) that all characteristic peaks do not alter for the disassembled PEO electrolytes after cycling, indicating that PEO is not oxidized during cycling due to the introduction of protective cPAN shell and the *in-situ* formed CEI layer. Moreover, XRD pattern of PEO electrolyte remains unchanged after long-term cycling, also confirming the unchanged structure of PEO even after cycling, as shown in Fig. S7. Fig. 7(b, c) show surface morphologies of the NCM@cPAN cathode plates before and after cycling. By comparison, the NCM particles maintain the spherical structures and keep good contact with the cathode additives even after long-term cycling, demonstrating the effective protecting effect of cPAN coating layer and CEI layer. In addition, XPS spectra was performed to study the alterations in chemical valences of Ni for NCM@cPAN cathodes before and after cycling with the cutoff voltage of 4.20 V, as displayed in Fig. 7(d). Regarding the uncycled cathodes, the peaks located at ~855.7 and ~853.9 eV are corresponding to Ni^{3+} and Ni^{2+}[40]. After cycling, the relative peak intensity of Ni^{2+} and Ni^{3+} keeps almost unchanged for the cycled NCM@cPAN cathode, further proving high stability of NCM cathode with restricted side reactions on account of the protective cPAN shell and CEI layer.

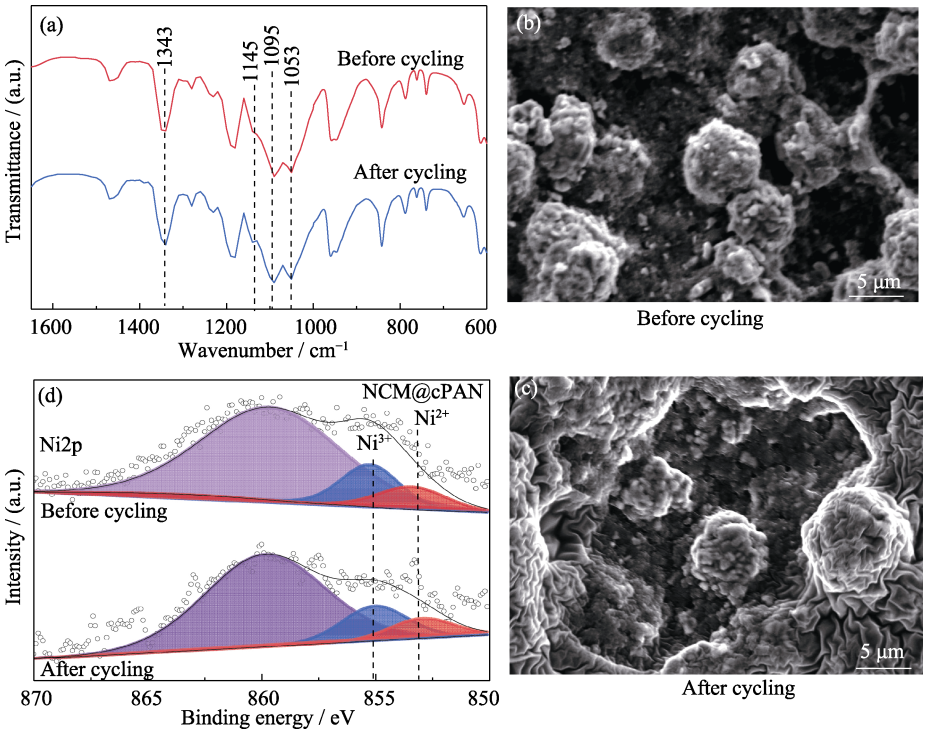

Fig. 7 (a) FT-IR spectra of PEO electrolyte before and after cycling; SEM images of NCM@cPAN cathodes (b) before and (c) after cycling; (d) Ni2p XPS spectra of NCM@cPAN cathode before and after cycling

3 Conclusions

The coupling of PEO solid electrolyte with high-voltage NCM cathode is achieved by surface coating of cPAN layer and interfacial introduction of ionic liquid. The cPAN layer with certain electronic transfer capability prevents the oxidation of PEO by physically separating PEO electrolyte from high-voltage NCM particles. The ionic liquid at cathode/PEO interface confirms the intimate interfacial contact, which is decomposed into an ionic conducting CEI consisting of LiF and Li_3N during cycling, contributing to the smooth Li^+ transfer at interface and further restricting the oxidation-failure of PEO electrolyte. By adopting such dual-strategy interface engineering, the solid-state NCM@cPAN+IL/PEO/Li cell delivers an excellent cycling stability after 100 cycles under the cutoff voltages of 4.20, 4.25 and 4.30 V. Moreover, a satisfactory areal capacity of 0.91 mAh·cm^{-2} is obtained when the cathode loading is increased to ~6.2 mg·cm^{-2}, along with a capacity retention of 86.2% after 50 cycles. This work provides a novel solution to achieve reliable stability of PEO-based electrolyte against high-voltage cathodes through the combination of surface coating and interface modification.

Supporting materials

Supporting materials related to this article refers to https://doi.org/10.15541/jim20230215.

References:

[1] CHENG X B, ZHANG R, ZHAO C Z, *et al.* Toward safe lithium metal anode in rechargeable batteries: a review. *Chemical Reviews*, 2017, **117(15):** 10403.

[2] LIU J, BAO Z, CUI Y, *et al.* Pathways for practical high-energy long-cycling lithium metal batteries. *Nature Energy*, 2019, **4(3):** 180.

[3] MA G, GUO L, DING X, *et al.* Effect of dual-functional electrolyte additive on high temperature and high voltage performance of Li-ion battery. *Journal of Inorganic Materials*, 2022, **37(7):** 710.

[4] XU H, SHI J, HU G, *et al.* Hybrid electrolytes incorporated with dandelion-like silane–Al_2O_3 nanoparticles for high-safety high-voltage lithium ion batteries. *Journal of Power Sources*, 2018, **391:** 113.

[5] COMMARIEU B, PAOLELLA A, DAIGLE J C, *et al.* Toward high lithium conduction in solid polymer and polymer-ceramic batteries. *Current Opinion in Electrochemistry*, 2018, **9:** 56.

[6] LI Y, MAO J, WEI C, *et al. In-situ* modification of carbon nanotubes with metallic bismuth nanoparticles for uniform lithium deposition. *Journal of Inorganic Materials*, 2022, **37(12):** 1337.

[7] WANG J, GE B, LI H, *et al.* Challenges and progresses of lithium-metal batteries. *Chemical Engineering Journal*, 2021, **420:** 129739.

[8] ZHANG H, DAI R, ZHU S, *et al.* Bimetallic nitride modified separator constructs internal electric field for high-performance lithium-sulfur battery. *Chemical Engineering Journal*, 2022, **429:** 132454.

[9] WEN Z, LIANG F. MOF/poly(ethylene oxide) composite polymer electrolyte for solid-state lithium battery. *Journal of Inorganic Materials*, 2021, **36(3):** 332.

[10] FAN L, WEI S, LI S, *et al.* Recent progress of the solid-state electrolytes for high-energy metal-based batteries. *Advanced Energy Materials*, 2018, **8(11):** 1702657.

[11] LIN D, YUEN P Y, LIU Y, *et al.* A silica-aerogel-reinforced composite polymer electrolyte with high ionic conductivity and high modulus. *Advanced Materials*, 2018, **30(32):** 1802661.

[12] ZHAO Y, ZHENG K, SUN X. Addressing interfacial issues in liquid-based and solid-state batteries by atomic and molecular layer deposition. *Joule*, 2018, **2(12):** 2583.

[13] WU J, RAO Z, CHENG Z, *et al.* Ultrathin, flexible polymer electrolyte for cost-effective fabrication of all-solid-state lithium metal batteries. *Advanced Energy Materials*, 2019, **9(46):** 1902767.

[14] CHEN R, LI Q, YU X, *et al.* Approaching practically accessible solid-state batteries: stability issues related to solid electrolytes and interfaces. *Chemical Reviews*, 2020, **120(14):** 6820.

[15] WAN Z, LEI D, YANG W, *et al.* Low resistance-integrated all-solid-state battery achieved by $Li_7La_3Zr_2O_{12}$ nanowire upgrading polyethylene oxide (PEO) composite electrolyte and PEO cathode binder. *Advanced Functional Materials*, 2019, **29(1):** 1805301.

[16] BALAISH M, GONZALEZ-ROSILLO J C, KIM K J, *et al.* Processing thin but robust electrolytes for solid-state batteries. *Nature Energy*, 2021, **6(3):** 227.

[17] LIU X Y, LIU B D, JIANG Y N, *et al. In-situ* synthesis of perovskite $SrTiO_3$ nanostructures with modified morphology and tunable optical absorption property. *Journal of Inorganic Materials*, 2019, **34(1):** 65.

[18] NIE K, WANG X, QIU J, *et al.* Increasing poly(ethylene oxide) stability to 4.5 V by surface coating of the cathode. *ACS Energy Letters*, 2020, **5(3):** 826.

[19] HUO H, CHEN Y, LUO J, *et al.* Rational design of hierarchical "ceramic-in-polymer" and "polymer-in-ceramic" electrolytes for dendrite-free solid-state batteries. *Advanced Energy Materials*, 2019, **9(17):** 1804004.

[20] YANG X, JIANG M, GAO X, *et al.* Determining the limiting factor of the electrochemical stability window for PEO-based solid polymer electrolytes: main chain or terminal –OH group? *Energy & Environmental Science*, 2020, **13(5):** 1318.

[21] YANG Q, HUANG J, LI Y, *et al.* Surface-protected $LiCoO_2$ with ultrathin solid oxide electrolyte film for high-voltage lithium ion batteries and lithium polymer batteries. *Journal of Power Sources*, 2018, **388:** 65.

[22] LIANG J, SUN Y, ZHAO Y, *et al.* Engineering the conductive carbon/PEO interface to stabilize solid polymer electrolytes for all-solid-state high voltage $LiCoO_2$ batteries. *Journal of Materials Chemistry A*, 2020, **8(5):** 2769.

[23] XU H, CHIEN P H, SHI J, *et al.* High-performance all-solid-state batteries enabled by salt bonding to perovskite in poly(ethylene oxide). *Proceedings of the National Academy of Sciences of the United States of America*, 2019, **116(38):** 18815.

[24] WANG Y, LIU B N, ZHOU G, *et al.* Improved electrochemical performance of $Li(Ni_{0.6}Co_{0.2}Mn_{0.2})O_2$ at high charging cut-off voltage with $Li_{1.4}Al_{0.4}Ti_{1.6}(PO_4)_3$ surface coating. *Chinese Physics B*, 2019, **28(6):** 068202.

[25] QIU J, YANG L, SUN G, *et al.* A stabilized PEO-based solid electrolyte *via* a facile interfacial engineering method for a high voltage solid-state lithium metal battery. *Chemical Communications*, 2020, **56(42):** 5633.

[26] FENG W, LI J, LIU H, *et al. In-situ* modification of ultrathin and uniform layer on $LiCoO_2$ particles for 4.2 V poly(ethylene oxide) based solid-state lithium batteries with excellent cycle performance.

Electrochimica Acta, 2022, **421:** 140473.
[27] LI Z, LI A, ZHANG H, *et al.* Interfacial engineering for stabilizing polymer electrolytes with 4 V cathodes in lithium metal batteries at elevated temperature. *Nano Energy*, 2020, **72:** 104655.
[28] FU F, ZHENG Y, JIANG N, *et al.* A dual-salt PEO-based polymer electrolyte with cross-linked polymer network for high-voltage lithium metal batteries. *Chemical Engineering Journal*, 2022, **450:** 137776.
[29] ZHOU W, WANG Z, PU Y, *et al.* Double-layer polymer electrolyte for high-voltage all-solid-state rechargeable batteries. *Advanced Materials* , 2019, **31(4):** 1805574.
[30] SUN Y, DONG H, XU Y, *et al.* Incorporating cyclized-polyacrylonitrile with $Li_4Ti_5O_{12}$ nanosheet for high performance lithium ion battery anode material. *Electrochimica Acta*, 2017, **246:** 106.
[31] SUN X L, LIU Z, CHENG Z L. Design and fabrication of *in-situ* N-doped paper-like carbon nanofiber film for thiophene removal from a liquid model fuel. *Journal of Hazardous Materials*, 2020, **389:** 121879.
[32] HONG Y, HU Q, DONG H, *et al.* N-doped carbon coated porous hierarchical MnO microspheres as superior additive-free anode materials for lithium-ion batteries. *Scripta Materialia*, 2022, **211:** 114495.
[33] HAMEDANI A A, OW-YANG C W, HAYAT SOYTAS S. Silicon nanocrystals-embedded carbon nanofibers from hybrid polyacrylonitrile-TEOS precursor as high-performance lithium-ion battery anodes. *Journal of Alloys and Compounds*, 2022, **909:** 164734.
[34] FENG W, LIU H, ZHAO M, *et al.* Improving interfacial stability by *in situ* protective layer formation in 4.2 V poly(ethylene oxide) based solid state lithium batteries. *Journal of Power Sources*, 2022, **523:** 231062.
[35] XIE Z, WU Z, AN X, *et al.* 2-Fluoropyridine: a novel electrolyte additive for lithium metal batteries with high areal capacity as well as high cycling stability. *Chemical Engineering Journal*, 2020, **393:** 124789.
[36] CHEN K, SUN Y, ZHAO C, *et al.* A semi-interpenetrating network polymer electrolyte membrane prepared from non-self-polymerized precursors for ambient temperature all-solid-state lithium-ion batteries. *Journal of Solid State Chemistry*, 2021, **296:** 121958.
[37] YAN C, YAO Y X, CHEN X, *et al.* Lithium nitrate solvation chemistry in carbonate electrolyte sustains high-voltage lithium metal batteries. *Angewandte Chemie International Edition*, 2018, **57(43):** 14055.
[38] LI T, ZHANG X Q, SHI P, *et al.* Fluorinated solid-electrolyte interphase in high-voltage lithium metal batteries. *Joule*, 2019, **3(11):** 2647.
[39] POLU A R, RHEE H W. Ionic liquid doped PEO-based solid polymer electrolytes for lithium-ion polymer batteries. *International Journal of Hydrogen Energy*, 2017, **42(10):** 7212.
[40] SONG G, ZHONG H, WANG Z, *et al.* Interfacial film $Li_{1.3}Al_{0.3}Ti_{1.7}PO_4$-coated $LiNi_{0.6}Co_{0.2}Mn_{0.2}O_2$ for the long cycle stability of lithium-ion batteries. *ACS Applied Energy Materials*, 2019, **2(11):** 7923.

正极包覆与界面修饰: 双策略改善聚氧化乙烯固态电解质对高电压正极稳定性

谭淑雨, 刘晓宁, 毕志杰, 万 勇, 郭向欣

(青岛大学 物理科学学院, 青岛 266071)

摘 要: 聚氧化乙烯(PEO)基固体电解质具有成本低、对锂稳定、易于大规模生产等优点, 是固态锂电池最有前途的固体电解质。然而, PEO 对高压正极不稳定, 严重限制了其在高能量密度领域的应用。本研究在 $LiNi_{0.6}Co_{0.2}Mn_{0.2}O_2$ (NCM)正极颗粒上部分包覆环化聚丙烯腈(cPAN)纳米层作为电子导电层, 在 NCM/PEO 界面上引入离子液体作为离子导电通道, 用以提高 PEO 与高压 NCM 正极的相容性。其中, cPAN 层不仅在物理上隔离了 PEO 电解质与 NCM 正极的直接接触, 而且 cPAN 中具有非局域的 $sp^2\,\pi$ 键, 有助于正极内部的电子传输。同时, 高离子电导率的离子液体的流动性较高, 可以充分润湿正极侧界面, 并在循环过程中分解为富 LiF 和 Li_3N 的 CEI 层, 进一步限制 PEO 电解质的氧化分解。基于上述复合策略的固态 NCM/Li 电池可在 0.1C (1C=0.18 A·g^{-1}), 4.30 V 截止电压下稳定循环 100 次, 且容量保持率可达 85.3%。本研究通过表面包覆和界面修饰, 为提高 PEO 基电解质对高压正极的稳定性提供了可行方案。

关 键 词: 聚氧化乙烯; 环化; 高电压正极; 界面工程; 固态锂电池

中图分类号: TM911 **文献标志码:** A

Supporting information

Jointing of Cathode Coating and Interface Modification for Stabilizing Poly(ethylene oxide) Electrolytes Against High-voltage Cathodes

TAN Shuyu, LIU Xiaoning, BI Zhijie, WAN Yong, GUO Xiangxin

(College of Physics, Qingdao University, Qingdao 266071, China)

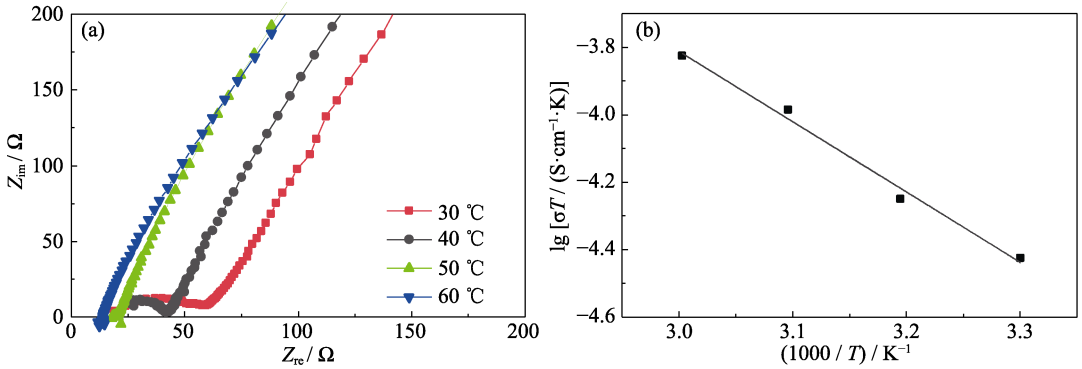

Fig. S1　(a) Nyquist plots of PEO-based electrolyte at different temperatures; (b) Arrhenius plot of PEO-based electrolyte

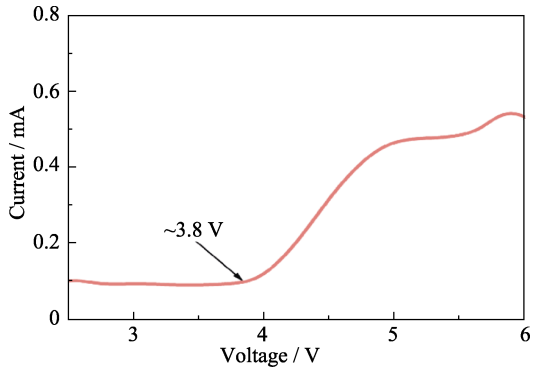

Fig. S2　LSV curve of PEO-based electrolyte

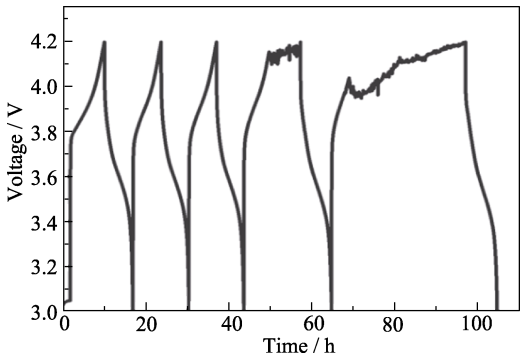

Fig. S3　Charge-discharge curve of NCM/PEO/Li batteries without IdiL at 50 ℃

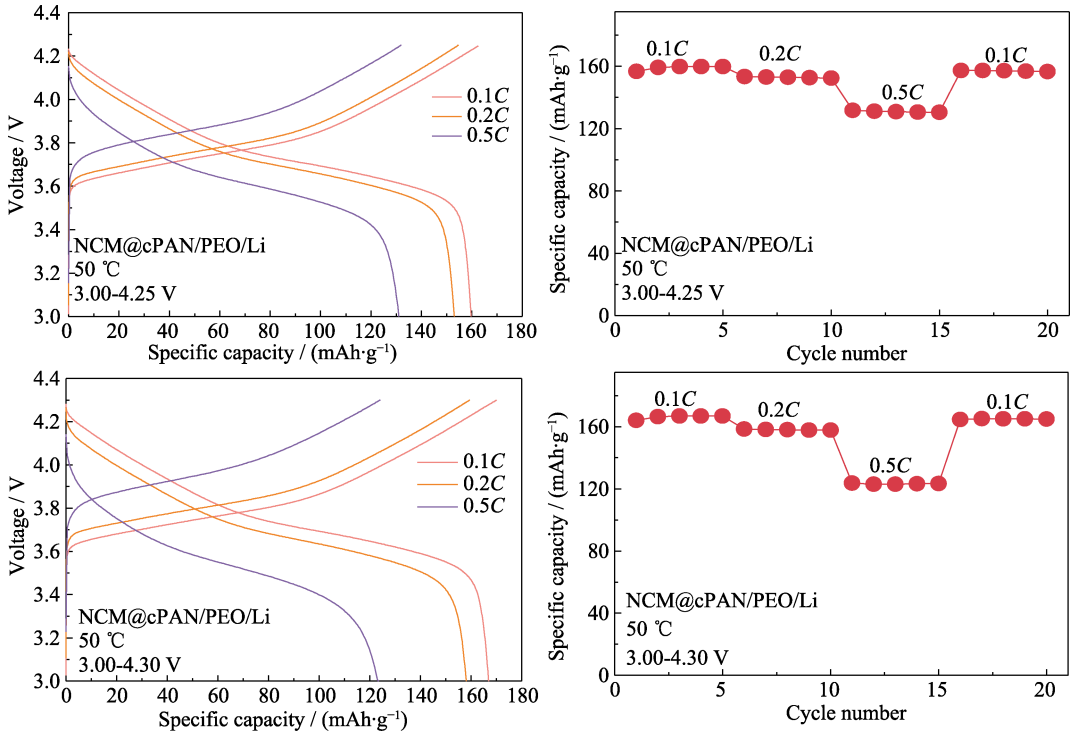

Fig. S4 Rate performance of solid NCM@cPAN+IL/PEO/Li batteries at various current densities

(a, c) Typical charge-discharge curves and (b, d) corresponding specific capacities with the cutoff voltages of (a, b) 4.25 V, and (c, d) 4.30 V

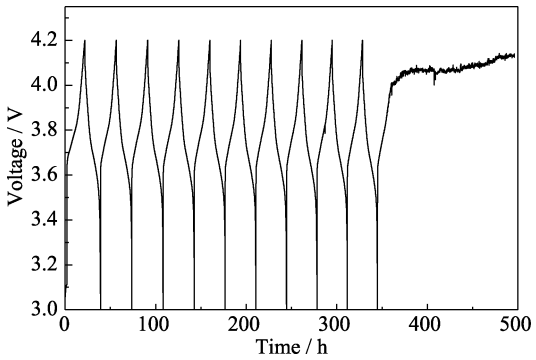

Fig. S5 Charge-discharge curve of NCM@cPAN/PEO/Li batteries without IL at 50 ℃

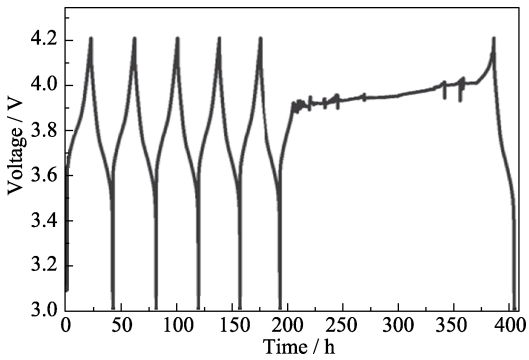

Fig. S6 Charge-discharge curve of NCM/PEO/Li batteries with IL at 50 ℃

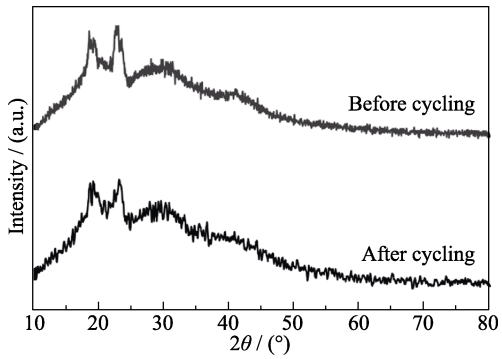

Fig. S7 XRD patterns of PEO electrolytes before and after cycling